

All-wheel drive electric vehicle modeling and performance optimization

Original

All-wheel drive electric vehicle modeling and performance optimization / de Carvalho Pinheiro, H.; Galanzino, E.; Messina, A.; Sisca, L.; Ferraris, A.; Airale, A. G.; Carello, M.. - In: SAE TECHNICAL PAPER. - ISSN 0148-7191. - ELETTRONICO. - 2019-36-0197:(2019). (Intervento presentato al convegno 2019 SAE Brasil Congress & Exhibition tenutosi a Sao Paulo, Brasil nel 14-18 October 2019) [10.4271/2019-36-0197].

Availability:

This version is available at: 11583/2816920 since: 2022-06-22T16:26:18Z

Publisher:

SAE International

Published

DOI:10.4271/2019-36-0197

Terms of use:

This article is made available under terms and conditions as specified in the corresponding bibliographic description in the repository

Publisher copyright

(Article begins on next page)

ALL-WHEEL DRIVE ELECTRIC VEHICLE MODELING AND PERFORMANCE OPTIMIZATION

H. de Carvalho Pinheiro, E. Galanzino, A. Messana, L. Sisca, A. Ferraris, A. G. Airale, M. Carello
Department of Mechanical and Aerospace Engineering, Politecnico di Torino - Italy

Abstract

Electrification of the powertrain is one of the most promising trends in the automotive industry. Among the novel architectures, this paper aims to study the latent advantages provided by in-wheel motors, particularly an All-Wheel-Drive powertrain composed by four electric machines directly connected to each wheel-hub of a high-performance vehicle. Beyond the well-known packaging advantage allowed by the in-wheel motor, the presence of four independent torque sources allows more flexible and complex control strategies of torque allocation. The study explores three different control modules working simultaneously: torque vectoring, regenerative braking and energy efficiency optimization protocol. The main objectives of the project are: improving handling, measured through the lap time of the virtual driver in a simulated track, and enhance energy efficiency, assessed by the battery state of charge variation during standard events. The torque vectoring strategy is based on a feedback PID controller working in parallel to a feedforward logic that predict the desired behavior based on the driver demands (such as steering angle) and vehicle states (chassis accelerations and velocities). The regenerative braking manages the demand of the driver by transferring decelerating torque from mechanical brakes to electric motors, based on their saturation condition, longitudinal slip of tires and the harmony with torque vectoring. Furthermore, a simulated 'engine braking' is developed and analyzed. The energy efficiency optimization protocol, allowed exclusively due to the presence of four independent electric motors, is an innovative approach to analyze the efficiency maps of the electric machines and find the best torque allocation in terms of power consumption without impact to longitudinal acceleration and yaw moment creation. The study successfully highlights the benefits of the all-wheel-drive in-wheel electric motors powertrain architecture and builds a solid platform to the development of the three control strategies and their relation, considering both the vehicle dynamics and the electric subsystem performance.

Introduction

Pure battery [1]-[2]- [3], hybridization [4]-[5]-[6], alternative fuels [7]-[8] and thermal propulsion systems (ICEs) are all likely to power vehicles to 2040 [9]. This is the conclusion of the report released by the Advanced Propulsion Center (APC) and produced on behalf of the United Kingdom's government-backed Automotive Council. However, electrification is undoubtedly recognized as the overarching technology that links them all.

For Electric Vehicles (EVs), motors, transmissions and associated controls will need to be integrated to achieve truly miniaturized, efficient packaging to reduce costs and enhance through-life efficiency and maintainability [9].

In-wheel motors have big potential to create an advanced all-wheel drive system for a full electric vehicle [10]. The increased complexity of the software to control each motor might be seen also as an opportunity to act directly on vehicle dynamics with a simplified powertrain from the mechanical point of view. This paper is developed in this direction: exploiting the advantage to directly control each wheel to increase the dynamic and energetic performance of the vehicle.

New mobility concepts for urban areas are leading to new vehicle concepts where mobility is being offered as a service in specially tailored business models. Drives that enable optimum use of space and a high degree of maneuverability, such as the wheel-hub drive (Figure 1), are taking center stage [11].



Figure 1 - Schaeffler's E-Wheel drive [11]

In-wheel motors have not succeeded yet in the automotive industry due to some reluctance shown by manufacturers. The main concern is caused by the increased unsprung mass. [12] A vehicle powered by in-wheel electric motors have a significant greater unsprung mass because the mass of a motor is in each powered wheel. Keeping unsprung mass low is fundamental both for lateral dynamics and ride comfort [13].

The most important advantage related to wheel-hub motors, which also represents the main reason why this EV layout was chosen for the research activity presented in this paper, is the possibility to deliver precisely controlled braking or motoring torque on a millisecond timescale [14]. If properly applied, this might lead to great improvements in traction and stability control, reducing stopping distances and enhancing drivability and safety. Torque vectoring, for instance, is a major implication related to dynamic stability and performance and, being one major goal of this paper.

A case study is proposed to verify the potential of this approach. Starting from a reference vehicle model (a high-performance racecar whose general characteristics are part of the standard VI-CarRealTime library) the main target is the development of a full electric powertrain and a control algorithm to regulate its correct functioning.

In order to achieve this goal a co-simulation environment is essential, since VI-CarRealTime standard powertrain is a central ICE and the In-wheel architecture under evaluation is not directly supported. The chosen interface to co-simulation was a Matlab-Simulink, that seamlessly interacts with VI-CarRealTime and allow sufficiently detailed modelling, control and data processing.

In this paper a theoretical background on wheel-hub electric motors and vehicle dynamics is provided, followed by a torque vectoring control theory discussion, taking into account that the torque vectoring was just one of the many methods introduced to distribute torque among the wheels. Its impact on vehicle dynamics was deeply assessed and performance improvements evaluated.

The modelling of the electric powertrain and the controller is also presented. Starting from the torque vectoring controller, all the energy saving algorithms, ranging from regenerative braking to power efficiency optimization protocol, are introduced together with their working principles. All the results obtained through simulations on VI-CarRealTime will be displayed and analyzed.

Theoretical Basis

Vehicle Dynamics

Starting from a rigid vehicle model, steady state high speed cornering considers the distribution of cornering forces between the axles and the side slip angles both vehicle and of each single wheel, without considering the internal dynamic behavior.

The vehicle model was considered like a monotrack (or bicycle) model (Figure 2), assuming the following assumptions:

- Vehicle speed $V = \text{constant}$;
- curved path with a high radius: $R \gg l, t$ (l is the wheel-base and t is the track of the vehicle);
- Aerodynamic forces and self-aligning torque are neglected;
- Vehicle and tires side slip angles are small.

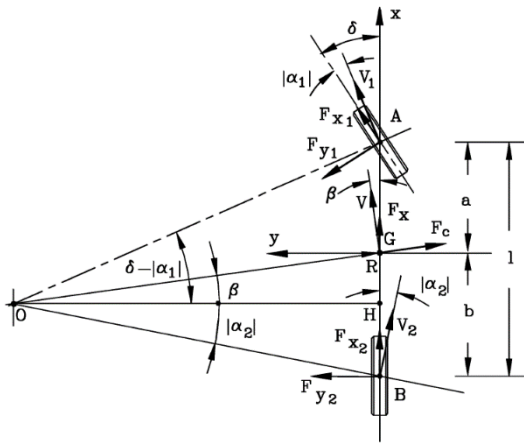


Figure 2 - Monotrack model [15]

A vehicle with four wheels can be described by a model with 10 degrees of freedom (6 + 2n equations of motion where n is the number of axles) neglecting the longitudinal slip of the wheels and the compliance of the steering system [15]. If the slips are considered, 14 DOF are necessary.

The equations obtained, however, are quite complicated nonlinear differential equations, difficult to write in explicit form. The solution of such set of equations can be computed by numerically integrating in time, starting from a given set of initial conditions and specifying the time history of the various inputs. A model of the driver to simulate the behavior of the vehicle-driver system has been used [15].

The choice of the simulation software has been very important, in particular VI-CarRealTime, because it operates in this way, based indeed on a 14 degrees of freedom model of the vehicle [16]:

- 6 DOFs from the vehicle chassis (sprung mass): 3 DOFs translations and 3 DOFs rotations
- 2 DOFs from each wheel (unsprung masses): 1 DOF for describing the motion with respect to the vehicle body and 1 DOF for the wheel longitudinal slip.

Torque Vectoring

To better understand the torque vectoring and how it influences lateral vehicle dynamics, a schematic representation of a cornering vehicle is shown in Figure 3 and Figure 4.

Equation 1 shows the correlation between yaw rate \dot{r} and yaw moment M_z :

$$J_z \dot{r} = M_z \quad (1)$$

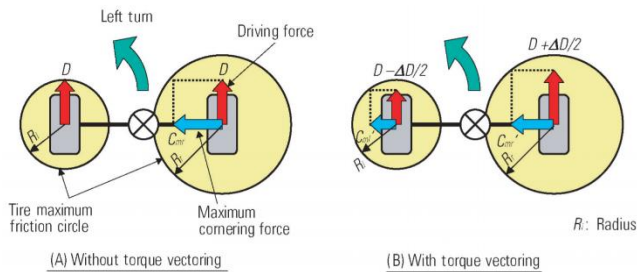


Figure 3 – Torque vectoring effect on driving forces between left and right wheel [17]

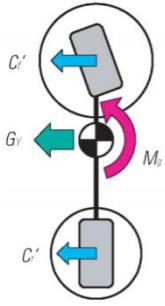


Figure 4 – Torque vectoring effect on yaw moment (adapted from [17])

The working principle of the torque vectoring is to distribute torque differently to each single wheel, in order to generate a yaw moment M_z which contributes to the vehicle cornering (Figure 4), in particular:

- TV is highly tunable to achieve better dynamic performance, energy efficiency or fun-to-drive characteristic;
- TV does not involve speed loss; on the contrary it helps in gaining speed during cornering. For this reason, in highly critical situations, active safety systems should intervene.

The main objectives of the TV are:

- Guarantee maximum longitudinal acceleration;
- Increase lateral dynamic performance in cornering;
- Distribute different torques to each electric motor to guarantee maximum energetic efficiency.

To generate yaw moment by means of torque vectoring, a control algorithm needs to be implemented, to generate a corrective yaw moment M_z , realizing than the Direct Yaw Control DYC. [18]

The theory behind the computation of the reference yaw rate is obtained through Equation 2:

$$\dot{\psi}_{\text{ref}} = r_{\text{ref}} = \frac{1}{R\delta} V\delta \quad (2)$$

Where: $1/R\delta$ is the curvature gain, V is the vehicle's speed and δ is the wheels' steering angle. V and δ are generated by the virtual driver and for the control system are inputs.

Regarding the actual yaw rate, it is usually computed based on a more complete 14 DOFs model of the vehicle.

For this paper, yaw rate DYC was also used, based on a PID feedback control with PID gains depending on vehicle's speed V . The PID controller used in the model computes the yaw rate error ε :

$$\varepsilon = r_{\text{ref}} - r_{\text{fb}} \quad (3)$$

Where: r_{ref} is computed with Equation 2 and $r_{\text{fb}} = r_{\text{actual}}$ computed with the 14 DOFs vehicle model (developed with VI-CarRealTime software).

Beside the feedback yaw rate control, a feedforward control was inserted in the model. This decision was taken to have a continuous reference yaw moment correction, generated by the feedforward. In this way, the feedback part of the controller, which is responsible for the creation of the precise yaw moment correction, acts in a smoother way because it is based on the reference feedforward signal [19][20].

The throttle percentage has been chosen between (-100%) and (+100%). This means that torque vectoring is working even at negative torque, helping to stabilize the vehicle also when driver's throttle demand is equal to zero or brakes are deployed. However, being the torques always applied by the electric motors, braking torques will not translate in a waste of energy as happening in the ESP system but will be converted in electric current to recharge the battery (regenerative braking).

Energy Optimization

In a 4WD full electric vehicle with wheel-hub motor, torques can be independently allocated to each electric motor. This means that the 4 degrees of freedom could be exploited. [21][22]

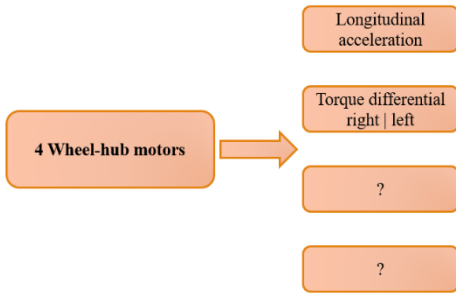


Figure 5 – Exploitable Degrees of Freedom

As shown in Figure 5, 2 DOF have already been used. The first DOF is exploited by the requested longitudinal acceleration, which imposes the total torque T_{tot} to be delivered by the four motors in the four wheels (T_{FR} , T_{FL} , T_{RR} e T_{RL}):

$$T_{tot} = T_{FR} + T_{FL} + T_{RR} + T_{RL} \quad (4)$$

The second DOF is instead needed for the torque differential imposed by the TV algorithm to generate the required yaw moment M_z :

$$M_z = \sum_i \frac{T_i}{R_e} \cos(\delta_i) y_i + \sum_i \frac{T_i}{R_e} \sin(\delta_i) x_i \quad (5)$$

The remaining DOF can therefore be used to have an optimal torque distribution, to guarantee an efficient usage of the electric motors from the energetic point of view.

One first step towards energy optimization was the implementation of a longitudinal slip limiter algorithm. To deeply understand the theoretical concept behind this idea, it is important to remember the correlation between the longitudinal force F_x exchanged between tires and ground and the longitudinal friction coefficient μ_x .

The higher the friction coefficient, the higher the maximum exchangeable force, and after this threshold a significant decrease in longitudinal force is observed, alongside with energy dissipation. Being the traction force directly proportional to the torque, it is important to exploit at the maximum the torque delivered by the motors, so that no energy is wasted.

To develop the traction control for slip reduction, a feedforward control was implemented in the model. This control reads as input the longitudinal slips of the wheels on front axle and compares it to those on the rear axle. If the slip difference between the two axles is above a certain threshold, it cuts the throttle on the axle with the highest slip.

A schematic representation of the control working principle for the slip reduction is shown in Figure 6.



Figure 6 – Traction control for slip reduction working method

The control algorithm works either during traction or during braking condition, and the two different situations can thus be outlined:

- Acceleration: due to load transfer, F_z on rear axle will increase, leading to an increase in the transmittable F_x . Leaving the same torque to be delivered to front and rear axle would cause a high slip on the front axle and a waste in energy; the throttle request to the front axle will therefore be limited.
- Braking: when regenerative braking is active, keeping the slip low would translate in a better exploitation of the braking force ($-F_x$) and, above all, reduce the risk of wheel slippage. In a similar way to the one described above, the regenerative torque would in this case be limited on the rear axle.

Still two DOF are available to better distribute torques among the wheel-hub motors. To this purpose, a second level controller was implemented in the model. Before precisely explaining the concept behind the power efficiency optimization algorithm, a schematic representation of the conceptual layout of the controller is shown in Figure 7.

The power efficiency optimization proposed aims to improve the overall efficiency of the system keeping each motor in the optimal operating point of its efficiency map.

Since many combinations of torque distributions need to be analyzed to find the optimal torque allocation, this operation is not doable in real-time. For this reason, the power efficiency optimization algorithm is based on a three-dimensional lookup table.

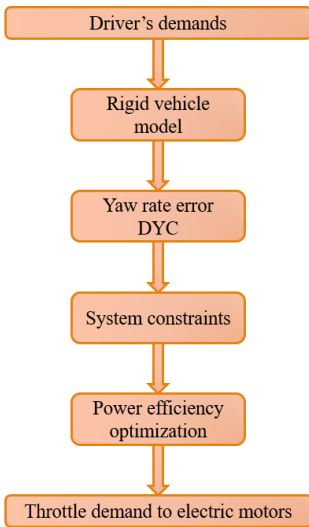


Figure 7 – Conceptual block scheme of the control model

The LookUp Table is created in Matlab to be afterwards exported into Simulink. It is a three-dimensional lookup table that it needs three input to generate an output. The inputs needed consist of those system constraints, which cannot be modified by the optimization algorithm, in particular:

- Total torque (longitudinal acceleration),
- Torque differential between left and right wheels (yaw rate),
- Wheels rotational velocity.

Given those inputs, the LUT provides the optimal torque to be delivered by one electric motor as output.

The LUT has been created in Matlab individuating each possible combination of torques at every inputs' values. A set of four torques is therefore chosen and associated to each group of inputs when the objective function is satisfied. The objective function used for this energy optimization control method [23] is:

$$y_{\min} = \frac{n \left(\frac{T_{FR} + T_{FL} + T_{RR} + T_{RL}}{\eta_{FR} \eta_{FL} \eta_{RR} \eta_{RL}} \right)}{n T_{\text{tot}}} \quad (6)$$

Where: T are the torques, n is the rotational velocity of the motors and η are the corresponding efficiencies.

The function needs to be minimized as it represents the ratio of the sum of the electric powers actually consumed by each motor to the power required for the electric vehicle to travel [23].

While Equation 6 refers to consumed power, a similar objective function was built to account for regenerative braking:

$$y_{\max} = \frac{n \left(\eta_{FR} |T_{FR}| + \eta_{FL} |T_{FL}| + \eta_{RR} |T_{RR}| + \eta_{RL} |T_{RL}| \right)}{n |T_{\text{tot}}|} \quad (7)$$

In this case, the function needs to be maximized as it represents the ratio of the sum of the electric powers regenerated by each motor to the maximum regenerable power.

In conclusion, the goal of these optimization functions is not to increase the single motor efficiency, but to improve the whole system efficiency finding an operating point that, in case of traction, minimizes the total electric power consumed and, in case of braking, maximizes the regenerated one.

Vehicle Model and Control Strategy

The general characteristics of the vehicle implemented in VI-CarRealTime are presented in Table 1.

Table 1 – Vehicle Race Car characteristics

Parameter	Value
Vehicle sprung mass (battery pack excluded) ms	1052 kg
Vehicle unsprung mass (wheel-hub motors included) mus	294 kg
Vehicle yaw moment of inertia (Izz)	1505211100 kg-mm ²
Wheelbase (l)	2713 mm
CG longitudinal front wheel distance (a)	1230 mm
CG height (hg)	381 mm
Front track width (tf)	1665 mm
Rear track width (tr)	1665 mm
Front cornering stiffness (Cfront)	306000 N/rad
Rear cornering stiffness (Crear)	348000 N/rad
Front tires overall radius	329 mm
Rear tires overall radius	353 mm

Table 2 – Motor characteristics

Parameter	Value
Peak output power	80 kW
Continuous output power	60 kW
Peak torque	1250 Nm
Continuous torque	650 Nm
Motor diameter	433 mm
Motor axial depth	125 mm
Motor mass	36 kg
Maximum speed	1600 rpm
DC supply voltage	400 V
Min ambient temperature	-40 °C
Max ambient temperature	+90 °C

This data will be used afterwards to build the rigid vehicle model to generate the reference yaw rate signal. The most relevant characteristics of the motor are reported in Table 2.

The data presented in Table 2 and Figures 8 and 9 are inserted in Simulink to model the electric powertrain. All the dynamic parameters of the electric motors are neglected because not provided by the manufacturer. However, being the dynamic response of modern electric motors much faster than wheel dynamics, its influence on vehicle dynamics can be considered not significant [24].

The torque vs. speed and the power vs. speed curves are provided respectively in Figure , while efficiency map is shown in 9.

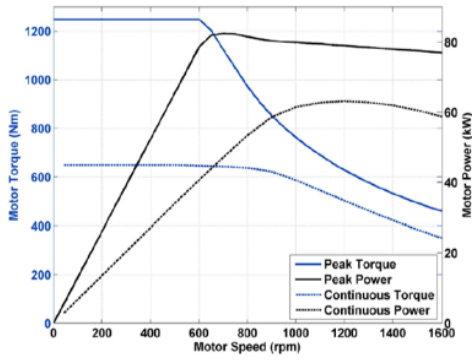


Figure 8 – Torque and Power vs. Speed [25]

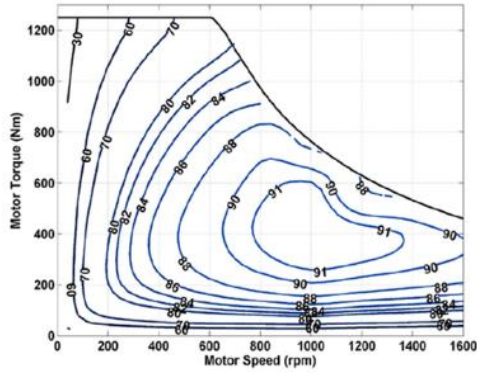


Figure 9 – Efficiency map [25]

A schematic representation of the control is displayed in Figure 1010.

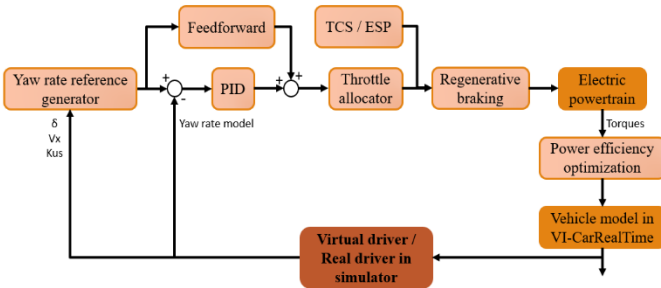


Figure 10 – Scheme of the controller

PID controller is a simple, yet very versatile and tunable feedback controller. It is a quite diffused controller for its effectiveness and its simple understanding. However, it can be seen as a sophisticated controller, as it is able to capture the history of the system through integrator and can anticipate the future behavior of the system through differentiator [26].

The output of the PID controller is calculate in the time domain with the equation:

$$u(t) = K_P e(t) + K_I \int e(t) dt + K_D \frac{de(t)}{dt} \quad (8)$$

Where: K_P is the proportional gain, K_I is the integral gain, K_D is the derivative gain and $e(t)$ is the feedback error.

Since the controller is working at different velocities, PID gains were chosen not to be fixed but to vary as function of speed. An adaptive PID control algorithm is therefore proposed; gains are updated as they are also updated as a function of the yaw rate error [19].

Regarding the first condition, it has been implemented to simulate the engine braking situation, which usually occurs in ICE equipped vehicles. When throttle is released, a regenerative braking, computed as throttle percentage, is applied to the vehicle to slow it down and recharge the battery. This braking action should not be too harsh; for this reason, regeneration percentage is limited as function of speed (the higher the speed, the higher the applicable braking percentage). Apart from the speed limitation, also a steering angle limit

was imposed, to avoid having an abrupt braking action during a curve. A Matlab script to compute the maximum regeneration percentage for engine braking, based on steering angle and steering angle derivative, was therefore created. Referring to the second condition, when a braking torque is applied, a simple algorithm will transfer the braking torque to the electric motors as long as they can handle it. If the braking torque is higher than the motor saturation limit, the torque in excess will be simply passed to the braking system. It is important to remember that torque vectoring is always operating, even during a braking maneuver, helping to stabilize the vehicle when braking in a curve.

In Simulink a subsystem dedicated to power optimization in created. Inside this block, four 3D lookup tables compute the desired torques based on:

- Wheels rotational velocity,
- Desired longitudinal acceleration,
- Desired yaw rate.

The lookup tables are computed by a Matlab script which, for each wheel, evaluate every possible torque, given a certain rotational velocity, yaw rate and longitudinal acceleration.

To simplify the script and reduce the computational time to calculate the 3D lookup tables, the assumption of equal rotational velocity $\Omega_{average}$ for all the wheels ($\Omega_{FR}, \Omega_{FL}, \Omega_{RR}, \Omega_{RL}$) was imposed. In this way, the three constraints could be used for every wheel. Wheels rotational velocity was therefore assumed to be equal to the average value:

$$\Omega_{average} = \frac{\Omega_{FR} + \Omega_{FL} + \Omega_{RR} + \Omega_{RL}}{4} \quad (9)$$

Since this assumption had been used in the lookup tables calculation, it was fundamental to impose it also for the computation of the optimized motors efficiencies, the electric power consumed and, consequently, the battery SOC. [27]

Simulation Results

Ramp Steer

Ramp steer maneuver was chosen to purely analyze the torque vectoring effects on the vehicle's lateral dynamics in an almost steady state condition. It is an open loop steering maneuver, which means that the steering angle is imposed and not controlled by the virtual driver. The driver only controls the throttle demand to assure that the target speed is always maintained.

Two ramp steer maneuvers were created (Table 3). For each ramp steer, base and performance driving modes were compared.

In the first ramp steer, the vehicle is distant from its limit condition; however, the effects of torque vectoring are already clearly visible.

Table 3 – Ramp steer manoeuvres characteristics

	Ramp steer 1	Ramp steer 2
Turn direction	Left	Left
Speed [km/h]	90	180
Ramp slope [deg/s]	6	3
Ramp duration [s]	10	10

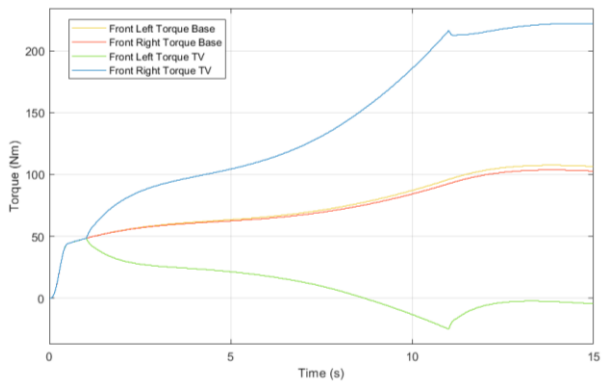


Figure 11 – Front left and front right wheel torques

As displayed in Figure , even negative torques can be requested. The difference between the base vehicle and the controlled one in terms of yaw rate and understeering gradient is shown in Figure 92 and Figure 103 respectively.

To better highlight the vehicle improved responsiveness, a second ramp steer at higher speed and higher lateral acceleration has been performed (Table 3).

Comparing Figure 103 to Figure 114, the increased lateral acceleration of the vehicle better highlights the difference between the base and the controlled one. Above 1g of lateral acceleration, the behavior of the base vehicle shifts towards a more understeering one. Torque vectoring instead helps in maintaining a linear relationship between the steering input and the lateral acceleration, improving the handling capability.

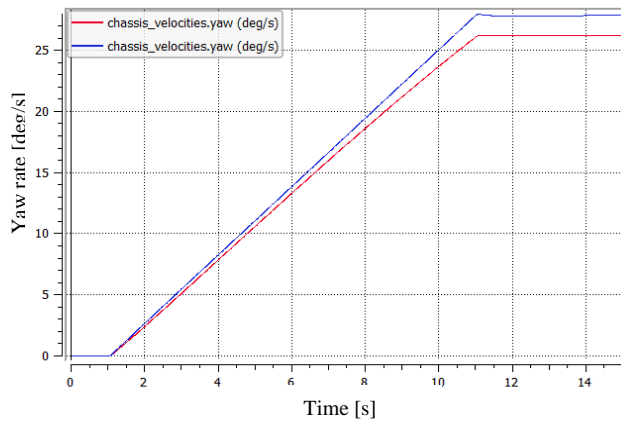


Figure 92 – Yaw rate comparison (red: base, blue: controlled)

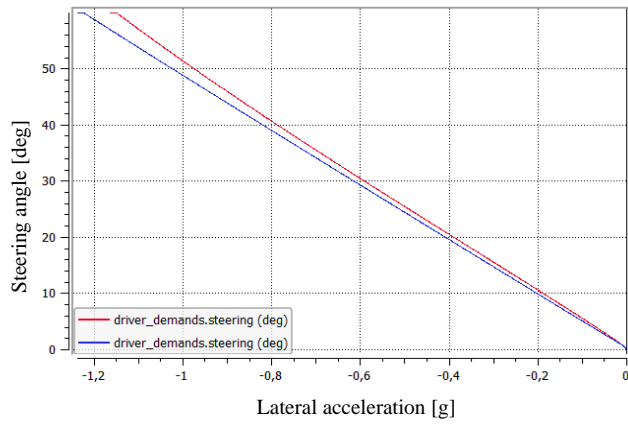


Figure 103– Wheel steering angle vs. lateral acceleration (red: base, blue: controlled)

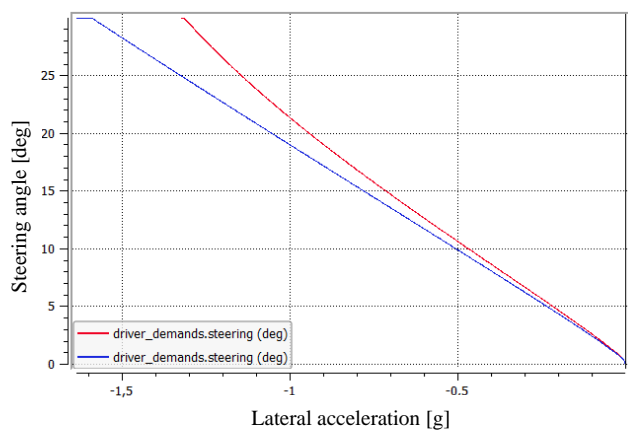


Figure 114 – Wheel steering angle vs. lateral acceleration (red: base, blue: controlled)

NEDC

The NEDC is a standard cycle to evaluate longitudinal performance of vehicles in terms of energy efficiency and fuel consumption. Table 4 presents the main characteristics of the NEDC and Figure 15 shows its speed profile, that should be followed by the testing vehicle. Table 4 – NEDC data [23]

Table 4 – NEDC data [23]

Time duration (s)	Distance (m)	Max speed (km/h)	Average speed (km/h)
1184	10932	120	33,23

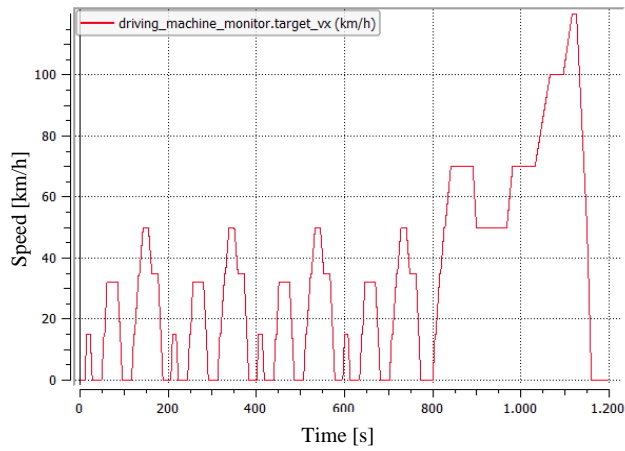


Figure 125 – NEDC cycle

NEDC cycle requires the vehicle to work at partial load, enhancing the motors efficiency influence on consumption.

Energy savings will be expressed in terms of SOC difference, with $SOC_{in}=90$. The results are reported in Table 5, that specify which energy optimization subsystem was active in each simulation. It is possible to note that energy savings are relevant both regarding regenerative braking and power efficiency optimization. The trends of the different SOC as function of the NEDC simulation time are presented in Figure 136.

Table 5 – Energy saving in NEDC cycle

	SOC	Δ SOC Base	$\Delta\%$ Base	km at Full Charge	Δ km Base
Base	87,23	0	0	355,2	0
Base + Regenerative braking	87,47	0,24	8,7	388,9	33,7
Base + Power efficiency optimization	87,53	0,30	10,8	398,3	43,1
Full ECO	87,81	0,58	20,9	449,3	94,1

When regeneration is applied, braking torques are not dissipated but converted in electric power recharging the batteries. During NEDC cycle braking torques are applied for short periods, therefore the SOC growth is not evident in the first part of Figure 136. However, during the last braking of the extra-urban cycle, a braking torque equal to 200 Nm is applied and the SOC increase is visible on the right-hand side of the same Figure.

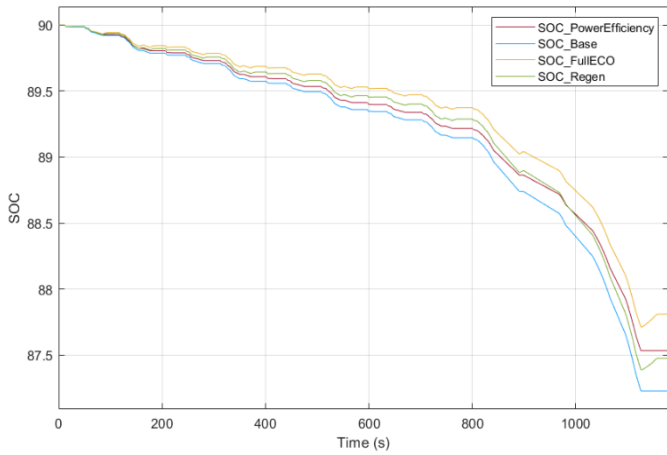


Figure 136 – SOC trend during NEDC cycle

Power efficiency optimization algorithm reveals to be highly effective in NEDC cycle. The motors always work at partial load, which represents a region of the efficiency map with lower efficiency. The power efficiency algorithm manages the torques on each wheel and, by moving it from rear to front axle, shifts the operational points to regions at higher efficiency.

Figure 147, Figure 158, Figure 169 and Figure 20 represent the efficiency and torque variation on each wheel. Only one wheel per axle has been plotted because, being the vehicle moving on a straight line, the torques are symmetrically distributed. Furthermore, only the last part of the NEDC cycle (extra-urban) has been plotted to obtain clearer graphs.

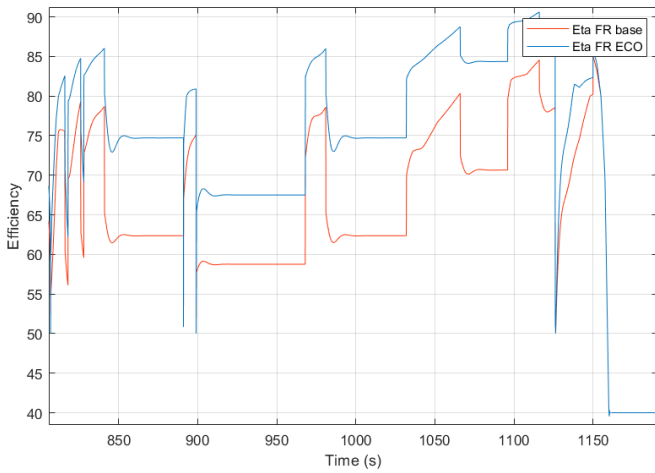


Figure 147 – Front-right wheel efficiency

In the plots, the red curve always refers to the baseline model, while the blue one corresponds to the controlled one. As highlighted in Figure 147 and Figure 158, the control increases the torque on the front wheel and, doing that, moves the working point to a higher efficiency. To respect the system constraints, the torque diminishes on the rear axle.

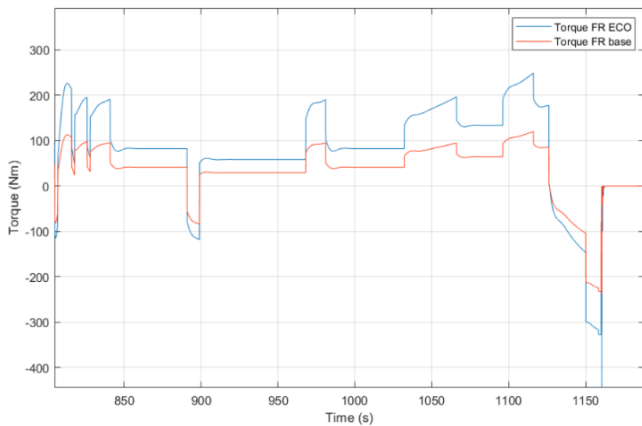


Figure 158 – Front-right torque efficiency

Figure 20 shows that the torque on rear axle was indeed set to zero. In this way, the whole electric power is drawn by front motors and the total system efficiency is increased.

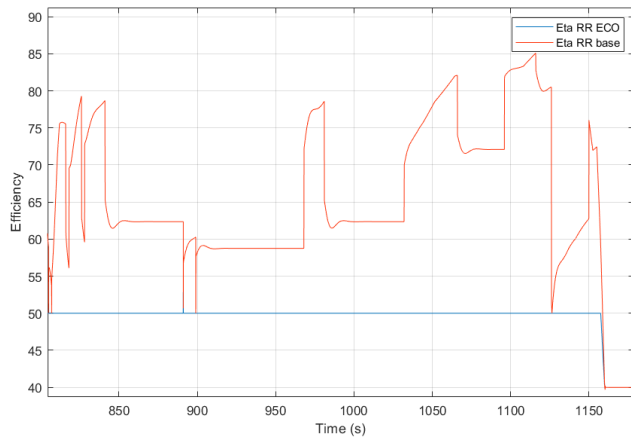


Figure 169 – Rear-right wheel efficiency

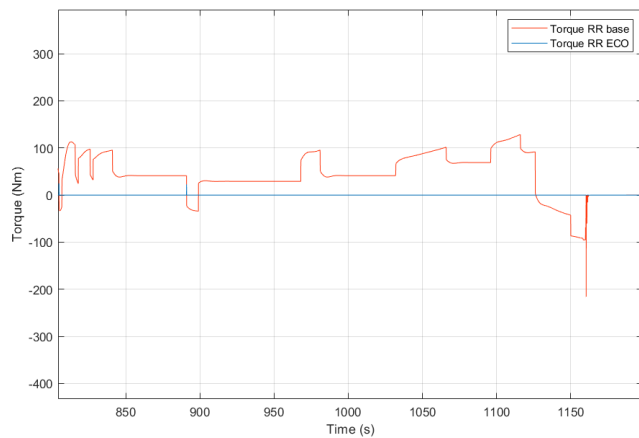


Figure 20 – Rear-right wheel torque

To better understand the idea behind this logic, Figure 171 represents the motor efficiency map with the base and ECO driving modes working point variation at 580 rpm (yellow dashed line, corresponding to the timestep $t=1000$ s in the NEDC cycle). The red line indicates the motors torque of the model without controller, equal on the four wheels. The point where it meets the yellow line represents the motor's operating point and the corresponding efficiency can be found looking at the blue lines (isoefficiency curves). The efficiency of the not controlled motors is therefore between 60% and 70%.

The green lines instead indicate the motors torque of the model with controller, which are different for the front (higher torque) and rear (lower torque) axle. Looking at the isoefficiency curves at the operating points (intersection with the yellow line), it can be noticed that the efficiency of the front motors working at higher torque is approximately equal to 80%. The rear torque is instead imposed to zero. The controller therefore shifted the whole torque on the front axle, obtaining a higher global efficiency.

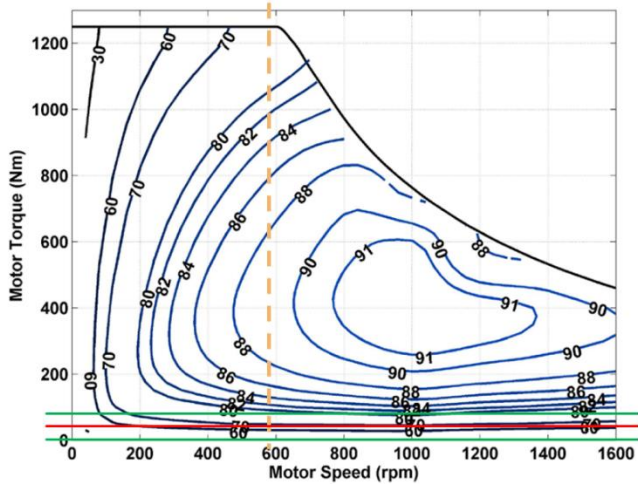


Figure 171 – Working points on efficiency map (red: base; green: ECO)

Racetrack

A flying lap time simulation on a race track was implemented both to address the torque vectoring dynamic performance improvements and to evaluate the energy saving algorithms in a more demanding driving condition compared to the NEDC cycle.

As suggested by VI-Grade engineers, the chosen racetrack is a short version of Hockenheim ring (Figure 182). This particular circuit includes high speed and low speed curves, to better judge torque vectoring behavior, and is approximately 2600 m long.

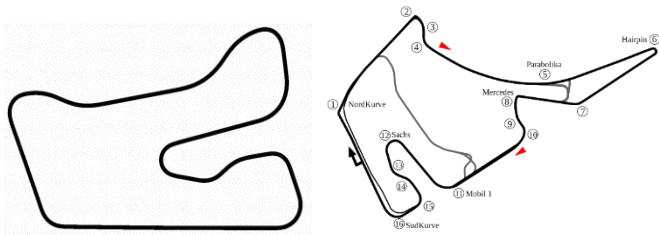


Figure 182 – Hockenheim ring short VI-Grade (left) and full Hockenheim ring

Flying lap time has proven to be a useful tool to evaluate performance gain given by torque vectoring implementation.

Table 6 – Lap time improvement

Driving mode	Lateral PF	Lap Time [s]	Δ Lap Time Base [s]	$\Delta\%$ Base
Base	1,10	63,271	0	0
Performance	1,16	62,620	-0,651	-1,03

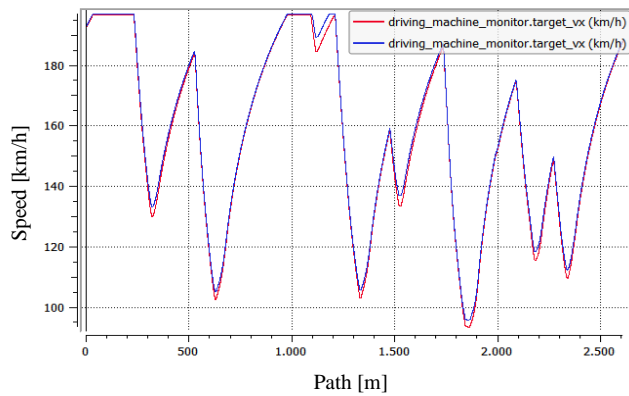


Figure 193 – Speed profile (red: base, blue: controlled)

Analyzing the speed profile of the two vehicles, it is clear how the controlled one has always higher speed when entering a curve (each local minimum in Figure 193). Indeed, as explained when discussing the ramp steer results, torque vectoring decreases the understeering behavior and enhances the response of the vehicle.

Energy saving potential was evaluated in a flying lap (FL) simulation and compared to the results obtained in the NEDC cycle. Table 7 and Table 8 present the results related to regenerative braking and power efficiency optimization algorithm respectively. Every simulation is performed at constant lap time, to verify the actual impact of energy saving algorithms without altering vehicle's performance. Before discussing the obtained results, it is important to specify that slip reduction algorithm based on traction control was not implemented during these simulations. Even if its impact on energy consumption was proved to be beneficial, this control compromises the vehicle's performance (and thus the lap time).

During a flying lap, braking torques are much greater compared to NEDC cycle. Braking request often reaches 100% and, if regeneration is active, electric motors are saturated. When working around saturation limit, motors operate at high efficiency (around 90%) and power regenerated is therefore high. Comparing the improvement in percentage points to the one obtained in NEDC cycle, it is noticeable how the potential electric power regenerable during a flying lap far exceeds that obtained in the driving cycle.

Referring to the power efficiency optimization algorithm, the results are reversed. Looking at Table 8, the SOC of the controlled vehicle is only 0.46% higher than the standard one. This is because, during a flying lap, throttle request is often equal to 100%, therefore the motors work at saturation limit with high efficiency. The energy saving gain is so weak that, if the assumption of equal rotational velocity for each wheel is not respected, the power optimization algorithm is not convenient in case of high-performance driving condition.

Table 7 – Energy saving in flying lap with regenerative braking

Driving mode	Lateral PF	SOC [FL]	Δ SOC Base [FL]	$\Delta\%$ Base [FL]	$\Delta\%$ Base [NEDC]
Base	1,10	84,97	0	0	0
Regenerative braking	1,10	85,98	1,01	20,08	8,66

Table 8– Energy saving in flying lap with ECO

Driving mode	Lateral PF	SOC [FL]	Δ SOC Base [FL]	$\Delta\%$ Base [FL]	$\Delta\%$ Base [NEDC]
Base	0,50	87,62	0	0	0
Power eff. optimization	0,50	87,63	0,01	0,46	13,44

Conclusions

The objective of this paper was to develop an electric powertrain and an innovative control algorithm to highlight the potential of Full Electric Vehicles equipped with in-wheel motors. The performance increase achieved through the controller application was evaluated both from the dynamic and energetic point of view.

Starting from a given VI-CarRealTime vehicle model, the electric powertrain was completely developed in Simulink. The interaction between the dynamic model and the powertrain was provided in a real-time co-simulation environment between Simulink and CarRealTime.

The control algorithm represents the real core of this paper. Starting from the idea of torque vectoring to enhance vehicle dynamics, a more complete control design including also energy optimization protocols was developed. The controller was evaluated based on three maneuvers:

- Ramp steer: to study torque vectoring performance in a standard steady state maneuver.
- NEDC cycle: to analyze energy savings obtained through regenerative braking and power efficiency optimization protocols in a standard cycle at partial load.
- Racetrack lap time: to evaluate the interaction between torque vectoring and energy algorithms in a high-performance maneuver.

Ramp steer maneuver highlighted a decreased understeering behavior of the vehicle, showing a linear relationship between steering angle and lateral acceleration up to the adherence limit. NEDC cycle had proven useful in underlining the effectiveness of the energy saving algorithms. Both regenerative braking and power efficiency optimization protocols decreased vehicle's energy consumption up to 20.9% globally. The algorithm based on electric motors efficiency optimization was particularly effective due to the unfavorable working condition of the motors at partial load.

The interaction between the various controllers was tested in the racetrack lap simulation. Torque vectoring allowed a reduction in lap time of 0.651 s (approx. 1%). Regenerative braking provided a battery consumption reduction of 20%, even better than NEDC cycle because of the higher braking torques. On the contrary, the efficiency optimization protocol did not prove to be highly effective in reducing energy consumption because of the already high motors efficiency during the flying lap. Vehicle's dynamic performance however was not compromised by the presence of the energy saving protocols.

References

1. Scavuzzo, S., Guerrieri, R., Ferraris, A., Airale, A.G. and Carello, M.: Alternative Efficiency Test Protocol for Lithium-ion Battery. International Conference on Environment and Electrical Engineering and 2018 IEEE Industrial and Commercial Power Systems Europe, IEEEIC/I. Palermo, 12-15 June (2018), DOI: 10.1109/IEEEIC.2018.8493664.
2. Cittanti D., Ferraris A., Airale, A.G., Fiorot, S., Scavuzzo S. and Carello M., "Modeling Li-ion batteries for automotive application: A trade-off between accuracy and complexity", International Conference of Electrical and Electronic Technologies for Automotive, Torino 15-16 June 2017, pp. 8, 2017, ISBN: 978-88-87237-26-9, DOI: 10.23919/EETA.2017.7993213.
3. De Vita A., Maheshwari A., Destro M., Santarelli M. and Carello M., "Transient thermal analysis of a lithium-ion battery pack comparing different cooling solutions for automotive applications", Applied Energy, Vol. 206, pp. 12, 2017, ISSN: 0306-2619, DOI: 10.1016/j.apenergy.2017.08.184.
4. Cubito, C., Rolando, L., Ferraris, A., Carello, M. and Millo, F., 'Design of the control strategy for a range extended hybrid vehicle by means of dynamic programming optimization'. IEEE Intelligent Vehicles Symposium (IV), Los Angeles, CA, USA 11-14 June, pp. 1234–1241 (2017), ISBN: 978-1-5090-4804-5, DOI: 10.1109/IVS.2017.7995881
5. Ferraris A., Airale A.G., Messina A., Xu S. and Carello M. 'The regenerative braking for a L7e Range Extender Hybrid Vehicle' International Conference on Environment and Electrical Engineering and 2018 IEEE Industrial and Commercial Power Systems Europe, IEEEIC/I. Palermo, 12-15 June (2018), DOI: 10.1109/IEEEIC.2018.8494000.
6. Carello, M., Ferraris, A., Airale, A. and Fuentes, F., 'City Vehicle XAM 2.0: Design and Optimization of its Plug-In E-REV Powertrain'. SAE International Congress, Detroit (Michigan) 8-10 April, pp. 11, (2014), DOI 10.4271/2014-01-1822.
7. Carello M., De Vita A. and Ferraris A., 'Method for Increasing the Humidity in Polymer Electrolyte Membrane Fuel Cell', Fuel cells, Wiley-Vch Verlag GmbH & Co. KGaA, Weinheim, pp. 8, ISSN: 1615-6854, DOI: 10.1002, 2016.
8. Ferraris, A.; Messina, A.; Airale, A.G.; Sisca, L.; de Carvalho Pinheiro, H.; Zevola, F. and Carello, M., 'Nafion® Tubing Humidification System for Polymer Electrolyte Membrane Fuel Cells'. Energies 2019, 12, 1773. DOI: 10.3390/en12091773
9. 'Advanced Propulsion Center roadmap'. [Online]. Available: <https://www.sae.org/news/2018/08/advanced-propulsion-center-future-propulsion-report>. [Accessed: 23-Jan-2019].
10. Wang J., Wang Q., Jin L. and Song C., 'Independent wheel torque control of 4WD electric vehicle for differential drive assisted steering', Mechatronics, vol. 21, no. 1, pp. 63–76, Feb. 2011.
11. Ag S. T. and Kg C., 'Schaeffler Symposium 2018', p. 200, 2018.
12. Vos R., Besselink I. J. M. and Nijmeijer H., 'Influence of in-wheel motors on the ride comfort of electric vehicles', Proc. 10th Int. Symp. Adv. Veh. Control AVEC10 22-26 August 2010 Loughb. U. K., pp. 835–840, 2010.
13. S. Xu, A. Ferraris, A. G. Airale, and M. Carello, 'Elasto-kinematics design of an innovative composite material suspension system', Mechanical Sciences, vol. 8, n. 1, pp. 11–22, feb. 2017, DOI: 10.5194/ms-8-11-2017.
14. Hilton A. W. and Hilton C., 'Protean Electric's In-Wheel Motors Could Make EVs More Efficient', IEEE Spectrum: Technology, Engineering, and Science News, 26-Jun-2018. [Online]. Available: <https://spectrum.ieee.org/transportation/advanced-cars/protean-electrics-inwheel-motors-could-make-evs-more-efficient>. [Accessed: 23-Oct-2018].
15. Genta G. and Morello L., 'The automotive chassis'. Dordrecht: Springer, 2009.
16. 'VI-CarRealTime 17.1 Documentation', p. 887, 2016.
17. Sawase K. and Ushiroda Y., 'Improvement of Vehicle Dynamics by Right-and-Left Torque Vectoring System in Various Drivetrainsx', p. 7.
18. Fu C., 'Direct Yaw Moment Control for Electric Vehicles with Independent Motors', p. 176.
19. Novellis L. D., Sorniotti A., Gruber P., and Pennycott A., 'Comparison of Feedback Control Techniques for Torque-Vectoring Control of Fully Electric Vehicles', IEEE Trans. Veh. Technol., vol. 63, no. 8, pp. 3612–3623, Oct. 2014.

20. De Novellis L., Sorniotti A., Gruber P., Shead L., Ivanov V., and Hoepfing K., 'Torque Vectoring for Electric Vehicles with Individually Controlled Motors: State-of-the-Art and Future Developments', *World Electr. Veh. J.*, vol. 5, no. 2, pp. 617–628, Jun. 2012.
21. Wong A., Kasinathan D., Khajepour A., Chen S.-K., and Litkouhi B., 'Integrated torque vectoring and power management framework for electric vehicles', *Control Eng. Pract.*, vol. 48, pp. 22–36, Mar. 2016.
22. De Novellis L., Sorniotti A., and Gruber P., 'Optimal Wheel Torque Distribution for a Four-Wheel-Drive Fully Electric Vehicle', *SAE Int. J. Passeng. Cars - Mech. Syst.*, vol. 6, no. 1, pp. 128–136, Apr. 2013.
23. Gang L. and Zhi Y., 'Energy saving control based on motor efficiency map for electric vehicles with four-wheel independently driven in-wheel motors', *Adv. Mech. Eng.*, vol. 10, no. 8, Aug. 2018. doi: 10.1177/1687814018793064
24. Tahami F., Kazemi R., Farhanghi S., and Samadi B., 'Fuzzy Based Stability Enhancement System for a Four-Motor-Wheel Electric Vehicle', *SAE Automotive Dynamics & Stability Conference and Exhibition*, 2002.
25. 'ProteanDrive', Protean. [Online]. Available: <https://www.proteanelectric.com/protean-drive/>. [Accessed: 23-Feb-2019].
26. 'Control Tutorials for MATLAB and Simulink - Introduction: PID Controller Design'. [Online]. Available: <http://ctms.engin.umich.edu/CTMS/index.php?example=Introduction§ion=ControlPID>. [Accessed: 24-Feb-2019].
27. Murnane, M. M. and Ghazel A., 'A Closer Look at State of Charge (SOC) and State of Health (SOH) Estimation Techniques for Batteries.' 2017.

Contact Informations

Henrique de Carvalho Pinheiro
 Department of Mechanical and Aerospace Engineering
 Politecnico di Torino
 Corso Duca degli Abruzzi 24, 10129, Torino, Italy
henrique.decarvalho@polito.it

Massimiliana Carello
 Department of Mechanical and Aerospace Engineering
 Politecnico di Torino
 Corso Duca degli Abruzzi 24, 10129, Torino, Italy
massimiliana.carello@polito.it

Acknowledgments

The authors would like to acknowledge VI-grade Italy Team: Alessio, Francesco and all the people who helped in the activities.

Definitions/Abbreviations

4WD	Four Wheel Drive
APC	Advanced Propulsion Center
DOF	Degree of Freedom
EV	Electric Vehicle
FL	Flying Lap
ICE	Internal Combustion Engine
LUT	Look-up Table
NEDC	New European Driving Cycle
PID	Proportional Integrative Derivative
SOC	State of Charge
TV	Torque Vectoring